Absorber Diameter Effect on the Thermal Performance of Solar Steam Generator

Prof. Dr. Karima Esmael Amori
Department of Mechanical Engineering
College of Engineering
University of Baghdad
Email: drkarimaa63@gmail.com

Rand Ahmed Adeeb
Department of Energy Engineering
College of Engineering
University of Baghdad
Email: a.rand82@yahoo.com

ABSTRACT

In this work, a convex lens concentrating solar collector is designed and manufactured locally by using 10 convex lenses (concentrator) of a diameter 10cm and one Copper absorber tube of a diameter 12.5mm and 1mm in thickness 1m length. Two axes manual Tracking system also constructed to track the sun continuously in two directions. The experiments are made on 17th of May 2015 in climatic conditions of Baghdad. The experimental data are fed to a computer program to solve the thermal performing equation, to find efficiency and actual useful energy. Then this data is used in numerical CFD software for three different absorber diameters (12.5 mm, 18.75 mm and 25 mm). From the results that obtained the maximum thermal efficiency for the collector of diameter 12.5mm equal to 82.3% is higher than that for the collector of 18.75 mm and 25 mm diameter. The maximum outlet temperature is found equal to (105°C, 93.9°C and 83.5°C) for collector absorber diameter equal to (12.5 mm, 18.75mm and 25 mm) respectively. The maximum mass flow rate 0.53 kg/hr when the solar radiation intensity equal to 899 W/m^2. The all-day collector efficiency varies with diameter and reaches to maximum value of (77.9%, 61.4% and 52.8) for collector diameter equal to (12.5 mm, 18.75mm and 25 mm) respectively.
Keywords: Steam Generator, Solar, Thermal Performance.

تاثير قطر الانبوب الماص على الاداء الحراري لمولد بخار شمسي

أ.د.كريمه اسماعيل عموري
قسم الهندسة الميكانيكية
كلية الهندسة / جامعة بغداد

رند احمد اديب
قسم هندسة الطاقه
كلية الهندسة / جامعة بغداد

الخلاصه

في هذا العمل تم تصنيع المركز الشمسي محليا باستخدام (10) عدسات محدبه, قطر الواحده منها يساوي (10 سم) , وانبوب من النحاس قطره (12.5 سم) وطوله (1 م) وسُمكه (1 ملم) كمستلم للاشعاع الشمسي المركزبواسطه العدسات. كما تم استخدام نظام تتبع ثنائي المحور لتتبع الشمس يدويا بصوره مستمره خلال فتره القياس. سُجلت النتائج العمليه في اليوم السابع عشر من شهر نيسان , في الظروف الجويه لمدينة بغداد. تم ادخال القيم العمليه الى الحاسبه بواسطه (CFD software)لحل المعادلات وايجاد الايداء الحراري لاقطار مختلفه للانبوب المستلم تساو (25ملم , 18.75 ملم ,12.5 ملم) ,حيث تم حساب كل

من الكفاءه, و الطاقه الحقيقه المفيده الكليه. من خلال النتائج تبين ان الكفاءه العظمى للمركز الشمسي ذو نصف القطر الذي يساوي 12.5 ملم تساوي 82.3% حيث كانت اعلى من الكفائه للحالتين ذات القطر الذي يساوي 18.75 ملم وكذلك 25 ملم. سجلت اعلى درجة حراره للماء بمقدار (105˚C, 93.9˚C, 83.5˚C). وكان اعظم معدل لتدفق المائع يساوي 0.53 kg/hr عند اشعاع شمسي مقداره 899 W/m^2. وجد ان اعلى معدل للكفاءه الكليه لليوم الواحد تساوي (52.8% and 61.4% , 77.9%,)بتغيير القطر للمستلم للشعاع بمقدار (25ملم , 18.75 ملم ,12.5 ملم) على التوالي.

الكلمات الرئسيه: مولد بخار, شمسي, اداء حراري

1. INTRODUCTION

With the increase of fossil fuel demand, the environmental pollution caused by burning of fossil fuels has been considered as an international problem. The stratospheric ozone depletion, the acid precipitation and the global warming are examples of environmental pollution. Renewable energies including, solar energy, wind energy, biomass, hydropower, geothermal energy are suggested to resolve the global warming problem and alleviate the potential of energy crisis, **Tyagi et al., 2009**. Solar energy is a large source of energy. The power from the sun intercept by the earth is approximately 1.8×10^{17} W. Solar energy could supply all the present and future energy needs of the world on a continuing basis. This makes it one of the most promising of the unconventional energy sources**, Aung** and**d Li, 2014**.

The first study about two-phase thermosyphon loop was done by, **McDonald, et al., 1977.** They studied the effect of changing the tilt angle of the loop and the temperature difference between the evaporator and the condenser in a single rectangular loop with R-11 and R-113 as working fluids. They found that the highest performance is achieved when the loop is horizontally oriented because the condenser is flooded with no dry out. **El-Ouederni, et al., 2008** studied experimentally the parabolic solar concentrator. They used an experimental device consist of a dish of 2.2 m opening diameter. The experimental results show that the temperature in the center of the disc is near to 400°C. **Gupta, et al., 2014** investigated experimentally the performance of convex lens concentrating solar power collector prototype in water heating applications. They found that the maximum efficiency obtained was 72% and 78%. They concluded that the convex lenses panels' prototype was more efficient than conventional panels.

The objective of this work is to directly produce steam using convex lenses to concentrate the solar radiation into a small area at the absorber surface. An estimation of the effect of change of inlet water temperature and effect of solar radiation on the production of the steam for two absorber fill ratios 0.75 and 1 will be accomplished. A mathematical model based on heat balance principle for different parts of the system is developed and then solved numerically to evaluate the fluid flow and thermal characteristics of the system under different conditions.

2. EXPERIMENTAL SETUP

The components of the experimental rig consists of convex lenses (Concentrator part) with receiver. It is also consists of supply tank and connecting pipes, shown in **Fig.1a** and **Fig.1b.** The concentrating part is used as presented in **Fig.2**. 10 pieces of Magnifying Glass lenses fixed in aluminum rectangular frame, and the specifications of the lenses are given in **Table 1.**

A copper tube acts as an absorber with diameter of (12.5 mm), and length of (1 m), black mat painted as shown in **Fig.1**.The absorber is covered by glass tube of (50 mm) in diameter, closed with cups from spherical rubber to isolate the absorber from the ambient condition and to reduce the thermal losses.

The water is fed to the absorber tube by one vertical cylindrical tank made of plastic shell of (2 mm) thickness. The tank has diameter of (29 cm), length of (34 cm) and capacity of (17.5 liter). Inlet water enter the tank from top hole with floating used to control the water level, and the bottom outlet point feeds the absorber with water shown in **Fig.3**. The external surface is well insulated by glass wool insulator of (2 cm) in thickness. Plastic pipes of (12.5 mm) diameter are used as connecting pipes between the components of the system. They covered by glass wool insulator and connect the supply tank, receiver and condenser with each other as closed loop. Fittings such as elbows, valve and bends are used as connecting parts.

The frame of the lenses is manufactured locally from two aluminum slides with length of (1 m) connected together and the lenses fixed between them as illustrated in **Fig.4**. The frame of the lenses is located at the top of another frame manufactured locally from aluminum with dimensions of (0.4m x 0.4m x 0.5m) black painted.

2.1 Measurements

In order to measure the absorber surface temperature and inlet and outlet temperatures of water, 10 thermocouples J (Iron - constant) type are used, for measuring the glass cover and ambient temperature one kind of thermocouple is used type-K . Thermocouples are attached near the focal point to measure the surface temperature of the absorber. Thermocouple is placed for the inlet and outlet water of the absorber shown in **Fig.5**. These thermocouples are joined to a selector switch in series with a digital reader **Fig6a**. Pro'sKit 3PK-6500 thermometer reader is used for type-K thermocouple with measuring range: (-50ºC ~ 750ºC) shown in **Fig.6b**. One thermocouple is used to measure the glass cover temperature. Solar radiation data is taken from the meteorological station in Baghdad for the test days. Wind data are gained from the meteorological station in Baghdad for the test days

3. DATA PROCESSING

The local useful energy is calculated at each focal point by the following equation:

$$Q_{useful(x)} = Q_{abs(x)} - Q_{loss(x)} \quad (1)$$

$$Q_{abs(x)} = (\tau\alpha) I_T A_a \quad (2)$$

$$Q_{loss(x)} = \pi\, D_g\, x\ \left[h_w\left(T_g - T_a\right) + \varepsilon_g\, \sigma\left(T_g^4 - T_{sky}^4\right)\right] \quad (3)$$

T_{sky} is the effective sky temperature calculated by the equation suggested by, **Beckman** and **Duffie, 2005.**

$$T_{sky} = 0.0552\ (T_a)^{\,1.5} \quad (4)$$

h_w Is the natural convective heat transfer coefficient from the outer surface of the glass tube to ambient air is calculated by the equation suggested by, **Mullick** and **Nanda, 1989**.

$$h_w = 4 V_w^{0.58} D_g^{-0.42} \quad (5)$$

The total useful energy is calculated by the sum of all the local useful energy.

$$Q_{useful(T)} = \sum_{1}^{10} Q_{useful(x)}$$

The mass flow rate of the system is calculated by:

$$\dot{m} = \frac{Q_{useful(T)}}{C_p \Delta T} \quad (6)$$

$$\Delta T = T_{out} - T_{in}$$

The local actual useful heat gain is calculated as:

$$Q_{u(x)} = A_a F_{R(x)} \left[I_T(\tau\alpha) - \frac{U_{L(x)}(T_{in} - T_a)}{C} \right] \quad (7)$$

where C is the concentration ratio calculated as:

$$C = \frac{Aperture\ area\ (A_a)}{surface\ area\ of\ the\ absorber\ (A_{abs})} \quad (8)$$

The aperture area is calculated as shown in **Fig.7a**:

No. of lens = 10
Diameter of lens = 10 cm
Height of the triangle = 4.4656 cm Shown in **Fig.7b**
Base of the triangle = 4.465 cm

No. of shaded area = (no. of lenses × 2) + 2
= 22

Area of sector $= \frac{1}{2}\theta r^2$

$\theta = in\ rad$

$\theta = 2 \times \tan^{-1} \frac{2.2325}{4.4656}$

= 53°

= 0.9271 rad

Area of the sector = $\frac{1}{2} \times 0.9271 \times 5^2$

= 11.5898 cm^2

Area of the triangle = $\frac{1}{2} \times 4.465 \times 4.4656$

= 9.9694 cm^2

Shaded area = 11.5898 – 9.9694

= 1.6203 cm^2

Area of all lenses = area of one lens * 10

$= \frac{\pi\ 10^2}{4} \times 10$
$= 785\ cm^2$

Total Actual area of lenses = $785 - (1.6203 \times 22)$
$= 749.3523\ cm^2$
$= 0.0749\ m^2$

Surface area of the absorber tube is calculated as:

$$A_{abs} = \pi D_{abs} L$$

a- For absorber tube with diameter (D_{abs} = 1.25 cm):

$$A_{abs} = 0.0125\ \pi\ m^2$$
$$C = 2$$

b- For absorber tube with diameter (D_{abs} = 1.875 cm):

$$A_{abs} = 0.01875\ \pi\ m^2$$
$$C = 1.3$$

c- For absorber tube with diameter (D_{abs} = 2.5 cm):

$$A_{abs} = 0.025\ \pi\ m^2$$
$$C = 1$$

The value of the local heat loss coefficient $U_{L(x)}$ is calculated by the equation suggested by, **Beckman** and **Duffie, 2005:**

$$U_{L_{(x)}} = \left(\frac{A_{abs}}{(h_w + h_{r,g-s})\ A_g} + \frac{1}{h_{r,abs-g_{(x)}}}\right)^{-1} \quad (9)$$

The radiation coefficient can be calculated from equation suggested by, **Beckman** and **Duffie, 2005.**

$$h_{r,g-s} = \varepsilon_g\ \sigma(\bar{T}^3) \quad (10)$$

The local radiation coefficient $h_{r,abs-g_{(x)}}$ between the absorber and glass cover is calculated as:

$$h_{r,abs-g_{(x)}} = \frac{\sigma(T_{abs(x)} + T_g)(T_{abs(x)}^2 + T_g^2)}{\frac{1-\varepsilon_p}{\varepsilon_p} + 1 + \frac{1-\varepsilon_g}{\varepsilon_g}\left(\frac{A_{abs}}{A_g}\right)} \quad (11)$$

The local heat loss coefficient based on the outside receiver tube diameter between the surrounding and the fluid is suggested by, **Beckman** and **Duffie, 2005**.

$$U_{\circ(x)} = \left[\frac{1}{U_{L_{(x)}}} + \frac{D_{abs,o}}{h_{i(x)}\ D_{abs,i}} + \frac{D_{abs,o}\ \ln(D_{abs,o}/D_{abs,i})}{2k_{abs}}\right]^{-1} \quad (12)$$

The local collector efficiency factor is calculated as:

$$F'_{(x)} = \frac{U_{\circ(x)}}{U_{L_{(x)}}} \tag{13}$$

a – For single phase region: ($h_i = h_1$)

$Nu_{(x)}$ Depends on the length of the heated surface, and the Grashof number defined by, **Ishi and Kataoka, 1984.**

$$Gr = \frac{g\beta\left(T_{abs,x} - T_f\right)x^3}{\left(\mu_l/\rho_l\right)^2} \tag{14}$$

$$Nu_{(x)} = 0.3(Gr\mathrm{Pr}_l)^{0.3}\left(\frac{D_{abs}}{x}\right) \tag{15}$$

$$h_{1(x)} = \frac{Nu_{(x)}\, k_l}{D_{abs}}$$

$$F''_{1(x)} = \frac{F_{R1(x)}}{F'_{1(x)}} = \frac{\dot{m}\, C_p}{A_a U_{L1(x)} F'_{1(x)}}\left[1 - e^{-\left(A_a U_{L1(x)} F'_{1(x)}/\dot{m}\, C_p\right)}\right] \tag{16}$$

$$F_{R1(x)} = F'_{1(x)} \times F''_{1(x)}$$

$$Q_{u1(x)} = A_a F_{R1(x)}\left[I_T(\tau\alpha) - \frac{U_{L1(x)}(T_i - T_a)}{C}\right] \tag{17}$$

b- For two phase region: ($h_i = h_b$)

$h_{b(x)}$ is the convection heat transfer coefficient for the fluid inside the absorber tube is assumed to be homogeneous pool boiling, and calculated by the equation proposed by, **Roshenow, 1952.**

$$h_{b(x)} = \frac{q_{b(x)}}{T_{abs(x)} - T_{sat}} \tag{18}$$

$$q_{b(x)} = \mu_l\, h_{fg}\left[\frac{g(\rho_l - \rho_v)}{\in}\right]^{\frac{1}{2}}\left[\frac{C_{pl}\,(T_{abs(x)} - T_{sat})}{0.01\, h_{fg}\, Pr^{1.7}}\right]^{1.8} \tag{19}$$

$$F''_{b(x)} = \frac{F_{Rb(x)}}{F'_{b(x)}} = \frac{\dot{m}\, C_p}{A_a U_{Lb(x)} F'_{b(x)}}\left[1 - e^{-\left(A_a U_{Lb(x)} F'_{b(x)}/\dot{m}\, C_p\right)}\right] \tag{20}$$

$$F_{Rb(x)} = F'_{b(x)} \times F''_{b(x)}$$

$$Q_{ub(x)} = A_a F_{Rb(x)}\left[I_T(\tau\alpha) - \frac{U_{Lb(x)}(T_i - T_a)}{C}\right] \tag{21}$$

The efficiency of the collector is calculated as:

$$Q_{u(Total)} = \sum Q_{u1(x)} + \sum Q_{ub(x)} \quad (22)$$

$$\eta = \frac{Q_{u(Total)}}{I_T A_a \times 10} \quad (23)$$

4. ERROR ANALYSIS

Thermal efficiency (η) is a function of different variables according to Eq. (24).

$$\eta = \eta(\Delta T, I_T, \dot{m}) \quad (24)$$

Based on the error analysis presented in, **Holman, 1989**. The percentage error of the collector efficiency is calculated as:

$$w_R = \left[\left(\frac{\partial R}{\partial x_1} w_1\right)^2 + \left(\frac{\partial R}{\partial x_2} w_2\right)^2 + \cdots + \left(\frac{\partial R}{\partial x_n} w_n\right)^2\right]^{1/2} \quad (25)$$

$$w_\eta = \left[\left(\frac{\partial \eta}{\partial \Delta T} w_{\Delta T}\right)^2 + \left(\frac{\partial \eta}{\partial I_T} w_{I_T}\right)^2 + \left(\frac{\partial \eta}{\partial \dot{m}} w_{\dot{m}}\right)^2\right]^{1/2}$$

where w_R is the uncertainty in the result and w_1, w_2, ... w_n are the uncertainty in the independent variables.

$$\frac{\partial \eta}{\partial \Delta T} = \frac{\dot{m} C_p}{I_T A_a} = \frac{1.95 * 10^{-04} * 4175}{945 * 0.0749} = 0.0110$$

$$\frac{\partial \eta}{\partial I_T} = -\frac{\dot{m} C_p \Delta T}{{I_T}^2 A_a} = -\frac{1.95 * 10^{-04} * 4175 * 73}{945^2 * 0.0749} = -8.4734 * 10^{-4}$$

$$\frac{\partial \eta}{\partial \dot{m}} = \frac{C_p \Delta T}{I_T A_a} = \frac{4175 * 73}{945 * 0.0749} = 4108.4$$

$$w_\eta = 0.0420$$

$$\frac{w_\eta}{\eta} = \frac{0.0420}{0.8007} = 5.24\%$$

5. NUMARICAL MODEL.

5.1 Mathematical Model

5.1.1 Geometry.

The geometry of the physical model shown in **Fig.9** is created in GAMBET, version (2.4.6). The model consists of circular absorber of 1m length, (12.5 mm, 18.75 mm and 25 mm) in diameter.

5.1.2 Mathematical assumptions.

1- The absorber properties do not changed with temperature.

2- The emissivity of the glass cover and absorber were assumed to be constant with temperature.

3- The flow within the collector absorber is considered to be unsteady, three-dimensional laminar natural convection.

4- In energy equation the viscous dissipation is neglected.

5- The Boussineq approximation is invoked for the fluid properties to relate density change to temperature change, and to couple in this way the temperature field to the flow field.

5.2 GOVERNING EQUATIONS.

The software (FLUENT 2.3.26) was used to solve the governing continuity, momentum and energy equations. The steady state solution has been obtained by numerically solving the three-dimensional form of the governing equations, these equations being written in terms of dimensional variables for the defined geometry and associated boundary conditions. The domain was defined in the global coordinate frame in which the solver carries out the calculations. **White, 1991.**

5.2.1 The continuity equation

$$\frac{1}{r}.\frac{d}{dr}\left(\rho_w\ r\ V_r\right)+\frac{1}{r}.\frac{d}{d\emptyset}\left(\rho_w V_\emptyset\ \right)+\frac{d}{dz}\left(\rho_{ref} V_z\right)=0 \qquad (26)$$

where: ρ_{ref} = water density at the reference temperature.

$V_r, V_\emptyset$ and V_z are the flow velocities components in the r,∅ and z direction respectively.

5.2.2 The momentum equation

r-component

$$\rho_{ref}\left(V_r\frac{dV_r}{dr}+\frac{V_\emptyset}{r}\frac{dV_r}{d\emptyset}+V_z\frac{dV_r}{dz}-\frac{V_\emptyset^2}{r}\right) = \frac{-dp}{dr}+\mu\left[\left(\frac{d}{dr}\left(\frac{1}{r}\frac{d}{dr}(rV_r)\right)\right)+\frac{1}{r^2}\frac{d^2\ V_r}{d\emptyset^2}+\frac{d^2\ V_r}{dz^2}+\frac{2}{r^2}\frac{dV_\emptyset}{d\emptyset}\right]\rho g_r \qquad (27a)$$

where : gr is radial gravitational acceleration and calculated as $g\ cos\emptyset\ cos\theta$

∅-component

$$\rho_{ref}\left(V_r\frac{dV_\emptyset}{dr}+\frac{V_\emptyset}{r}\frac{dV_\emptyset}{d\emptyset}+v_z\frac{dV_\emptyset}{dz}-\frac{V_rV_\emptyset}{r}\right)=\frac{-dp}{d\emptyset}+\mu\left[\left(\frac{d}{dr}\left(\frac{1}{r}\frac{d}{dr}(rV_\emptyset)\right)\right)+\frac{1}{r^2}\frac{d^2\ V_\emptyset}{d\emptyset^2}+\frac{d^2\ V_\emptyset}{dz^2}+\frac{2}{r^2}\frac{dV_\emptyset}{d\emptyset}\right]+\rho g_\emptyset \qquad (27b)$$

where: $g_\emptyset$ is the circumferential gravitational acceleration, its determined as $g\ sin\emptyset\ cos\theta$

z-component

$$\rho_{ref}\left(V_r\frac{dV_z}{dr}+\frac{V_\emptyset}{r}\frac{dV_z}{d\emptyset}+V_z\frac{dV_z}{dz}-\frac{V_z\,dV_z}{dz}\right) = \frac{-dp}{dz}+\mu\left[\left(\frac{d}{dr}\left(\frac{1}{r}\frac{d}{dr}\left(\frac{dV_z}{dr}\right)\right)\right)+\frac{1}{r^2}\frac{d^2\ V_z}{d\emptyset^2}+\frac{d^2\ V_z}{dz^2}\right]+\rho g_z \qquad (27c)$$

where: gz is gravitational acceleration in z direction it is evaluated as $g\ sin\theta$

5.2.3 The energy equation

$$\rho_{ref} C_p \left(V_r \frac{dT}{dr} + \frac{V_\emptyset}{r}\frac{dT}{d\emptyset} + V_z \frac{dT}{dz}\right) = k\left[\frac{1}{r}\frac{d}{dr}\left(r\frac{dT}{dr}\right) + \frac{1}{r^2}\frac{d^2T}{d\emptyset^2} + \frac{d^2T}{dz^2}\right] \quad (28)$$

$$\rho = \rho_{ref}\left[1 - \beta\left(T - T_{ref}\right)\right] \quad (29)$$

5.2 Boundary Conditions and Modeling Specifications.

The boundary conditions are assigned for inlet velocity, inlet temperature, wall's heat flux and outlet pressure. The inlet velocity assumed to be equal to 10^{-5} m/s just to run the program. Inlet temperature data and wall heat flux are listed in **Table 2**. Pressure outlet boundary conditions required the specification of the static (gage) pressure at the outlet boundary. The value of static pressure assumed to be uniform atmospheric pressure since the pipe is open to ambient conditions.

5.3 Fluent Code

In this work FLUENT version 6.3.26 is used. FLUENT is a computational fluid dynamics (CFD) software package to simulate fluid flow and heat transfer problems. It uses the finite volume method to solve the partial differential equations of fluid flow and heat transfer. It provide the capability to use different physical models such as incompressible or compressible, in viscid or viscous, laminar or turbulent flow, and thermal or adiabatic heat transfer.

A mesh is used to reach to the correct converged solution that captures all the key parameters of the simulation. For the current simulation, enough nodes are needed to be placed near the boundaries to capture boundary layer flow, as well as the temperature gradient. Using too many nodes in the system may increases the computational resources and execution time without providing additional resolution. The details of the adopted mesh are: Interval Size of (Wall, inlet, outlet) Edges = 0.0004 cm, Growth Rate = 1.2 and Maximum Size = 0.001 cm. The mesh of the system is shown in **Fig.8**.

6. RESULTS AND DISCUSSION

Fig.10 shows that the efficiency of the system increases with the decreasing of the absorber diameter on 17th of May 2015. [I.e. the efficiency for the case of diameter equal to (12.5mm) was 12.1% higher than that for absorber with diameter of (18.75mm) and 30.3% higher than that for absorber of diameter equal to (25 mm).

Fig.11 shows that the useful energy of the system increases with the decreasing of the absorber diameter on 17th of May 2015. The useful energy for the case of diameter equal to (12.5mm) was 17.7% higher than that for absorber with diameter of (18.75mm) and 32.3% higher than that for absorber of diameter equal to (25 mm), due to the higher heat fluxes.

Fig.12 illustrates that the outlet temperature of the absorber (with diameter of 12.5, 18.75, and 25mm) increases from the first hour of the day to reach maximum value of (105 , 93.9, and 83.5°C) respectively at solar noon then decreased after that. This figure also shows that the outlet temperature increases with the decreasing of the absorber diameter.

Fig.13 Shows that the heat flux decreasing with the increasing of absorber size, because of the increasing of the surface area that the useful energy divided by it. The heat flux for the absorber diameter of (12.5 mm) was 33.2% higher than that for absorber with diameter of (18.75 mm) and 50% higher than for absorber with diameter of (25 mm) mm.

Fig.14 reports the mass flow rate for all three cases of (12.5, 18.75, and 25mm) increasing from the beginning of the day to reach maximum value of (0.53, 0.51 and 0.5 kg\hr) respectively at solar noon then decreased after that, due to large amount of evaporation in the system with the case of small diameter.

Fig.15 presents the daily efficiency for three different cases of absorber diameter of (12.5, 18.75, and 25 mm). It is increases with the decreasing of absorber diameter as (82.5, 70.2, and 58%) respectively.

Fig.16 shows the variation of outlet temperature with solar radiation for three different absorber sizes. It can be noticed that the outlet temperature in the case of (12.5mm) diameter was 10.45% higher than in case of (18.75mm) and 20.47% in case of (25mm) for the same solar radiation due to the smaller surface area produced larger heat flux.

Fig.17 illustrates the effects of absorber size variation on the useful energy, for same solar radiation. the useful energy at 13:00 PM was (48.19 , 39.66 and 32.78 W) for absorber diameters of (12.5, 18.75 and 25 mm) respectively for same amount of solar radiation equal to 899 W/m^2, because of the differences between inlet and outlet temperature and mass flow rate in case of the small diameter was higher than that for cases of large diameter.

Fig.18 shows the effect of the variation of the absorber diameter on the value of heat flux, for same solar radiation the heat flux increases with the decreasing of the absorber diameter. The heat flux at 13:00 PM was (1477.7, 986.13, and 738.8 W/m^2) for absorber diameter of (12.5, 18.75 and 25 mm) respectively for same amount of solar radiation equal to 899W/m^2.

7. CONCLUSIONS

The conclusions extracted from this work are:

1. Outlet temperature of the system increased about 10.45% and 20.47% with the decreasing of absorber size from (18.75 mm) and (25 mm) to (12.5 mm) for the same amount of solar radiation and useful energy.
2. The maximum value of outlet temperature for absorber tube with diameters equal to (12.5 mm, 18.75mm and 25 mm) were (105°C, 93.9°C and 83.5°C) respectively on 17th of May 2015.
3. The mass flow rate decreased with increasing of absorber diameter. The maximum value of mass flow rate reported was about (0.53 kg/hr.) at solar noon for collector with absorber diameter equal to (12.5mm).
4. The calculated heat flux subjected on the absorber surface increases with decreasing its diameter for same amount of incident solar radiation. For three different absorber diameters of (12.5, 18.75, and 25 mm) the maximum heat flux were (1477, 986, and 738 W\m^2) respectively for the same amount of incident solar radiation of 899W/m^2.

5. For two axes manual tracking system the average efficiency reached during the day was about (77.9, 61.4, and 52.8%) for collector diameter equal to (12.5, 18.75 and 25 mm) respectively.

REFERENCES.

- -Aung N. Z., and Li S., 2013, *Numerical Investigation on Effect of Riser Diameter and Inclination of System Parameters in a Two-Phase Close Loop Thermosyphon Solar Water Heater*, Energy Conversion and Management, Vol.75, pp. 25-35.

- -Beckman W. A, and Duffie J.A., 2005, *Solar Engineering of Thermal Process*, Wiley Interscience Publications, John Wiley & Sons, New York.

- -El-Ouederni A. R., Dahmani A. W., Askri F., Salah M. B, Nasrallah S. B., 2008 , *Experimental Study of a Parabolic Solar Concentrator*, Renewable Energies proceedings CICME' 08 source, pp. 193-199.

- -Gupta A. K., Gehlot D., Gujrathi A. S., 2014, *Experimental Investigation of Convex Lens Concentrating Solar Power Collector Prototype Performance*, International Journal of innovation in Engineering Research and Management, Vol.1, Issue.2, pp.193-199.

- -Grald E. W., Kuehn T. H., 1989, *Performance Analysis of a Parabolic Trough Solar Collector with a Porous Absorber Receiver*, Solar Energy, Vol. 42, pp. 281-292.

- -Howell J. R., Bannerot R.B., Vliet G.C., 1983, *Solar Thermal Energy System and Design*, McGraw-Hill Book Company, New York.

- -Holman J.P., 1989, *Heat Transfer*, fifth edition McGraw-Hill.

- -Ishii M., Kataoka I., 1984, *Scaling Laws for Thermal-Hydraulic System Under Single-Phase and Two-Phase Natural Circulation*, Nuclear Engineering and Design, Vol. 81, pp.411-425.

- -Joudi K. A., Al-tabbakh A. A., 1999, *Computer Simulation of a Two Phase Thermosyphon Solar Domestic Hot Water Heating System*, Energy conversion and management, Vol.40, pp. 775-793.

- -Lin M., Sumathy K., Dai Y. J., Zhao X. K., 2014, *Performance Investigation on a Linear Fresnel Lens Solar Collector Using Cavity Receiver*, Solar Energy, Vol.107, pp.50-62.

- -McDonald T. W., Huang K. S., Diciccio R., 1977, *Thermosyphon Loop Performance Characteristics Part 1*, Experimental study, ASHRAE Trans., Vol. 83, pp. 250-259.

- -Mullick S.C., and Nanda S.K., 1989, *An Improved Technique for Computing the Heat Loss Factor of a Tubular Absorber*, Solar Energy, Vol. 42, Issue 1, pp. 1-7.

- -Mohamad A., Orfi J., Alansary H, 2014, *Heat Losses From Parabolic Trough Solar Collectors*, International Journal of Energy and Research, Vol.38, pp. 20-28.
- -Rohsenow W. M., 1952, *A Method of Correlating Heat Transfer Data for Surface Boiling Liquids*, Trans. ASME, Vol.74, pp. 969-976.
- -Shuai Y., Xia X. L., Tan H. P., 2008, *Radiation Performance of Dish/Cavity Receiver Systems*, Solar Energy, Vol.82, pp.13-21.
- -Tyagi H., Phelan P., Prasher R., 2009, *Predicted Efficiency of a Low-Temperature Nanofluid–Based Direct Absorption Solar Collector*, Journal of Solar Energy Eng. 131, 041004.
- -Vincent C. C. J, and Kok J. B. W., 1992, *Investigation of the Overall Transient Performance of the Industrial Two-Phase Closed Loop Thermosyphon*, International Journal Heat Mass Transfer, Vol.35, No.6, pp.1419-1426.
- -White F.M., 1991, *Viscous Fluid Flow*, second edition, McGraw-Hill, Inc.

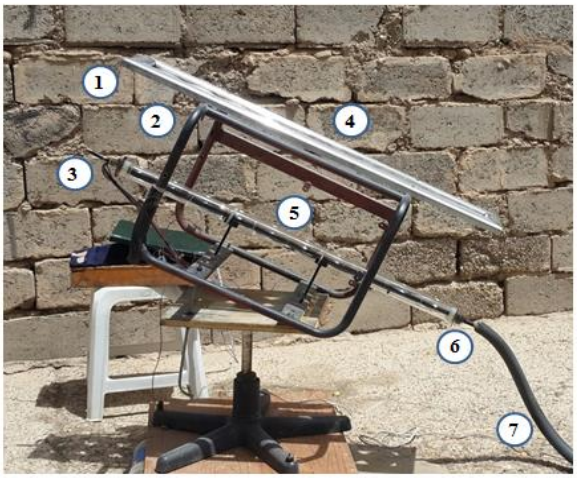

Figure 1a. Photograph for the outdoor testing set up.
1. Frame structure of the lenses.
2. Frame structure of the collector.
3. Outlet point.
4. Concentrating part.
5. Receiver (copper tube + glass cover).
6. Inlet point.
7. Connecting pipe.

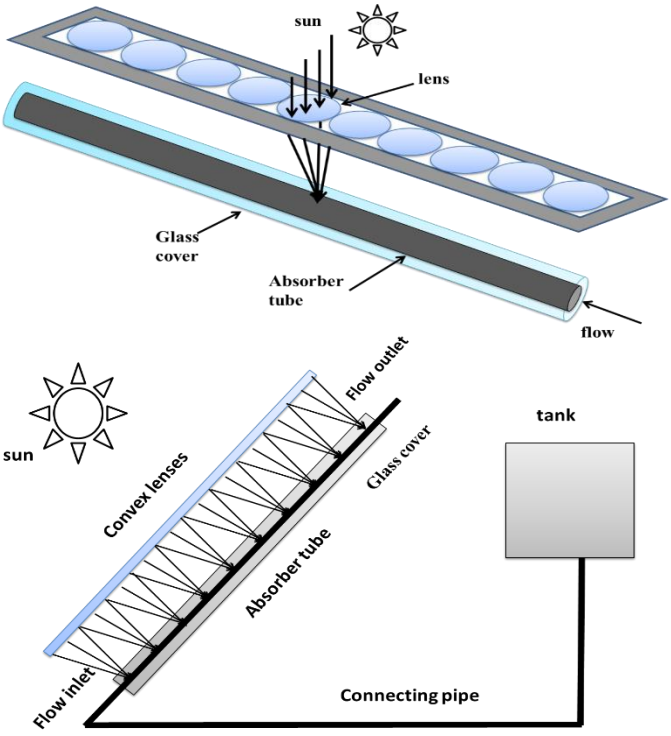

Figure 1b: Schematic diagram for the natural circulation concentrated solar collector.

Figure 2. Concentrating part (convex lenses).

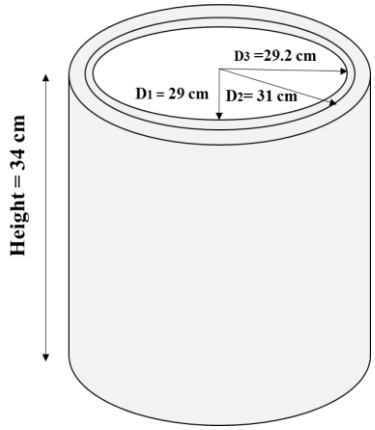

Figure 3. Schematic diagram for the supply tank.

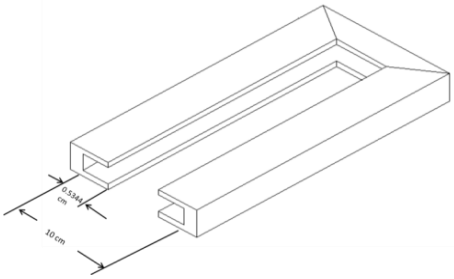

Figure 4. Schematic diagram of the frame of the lenses

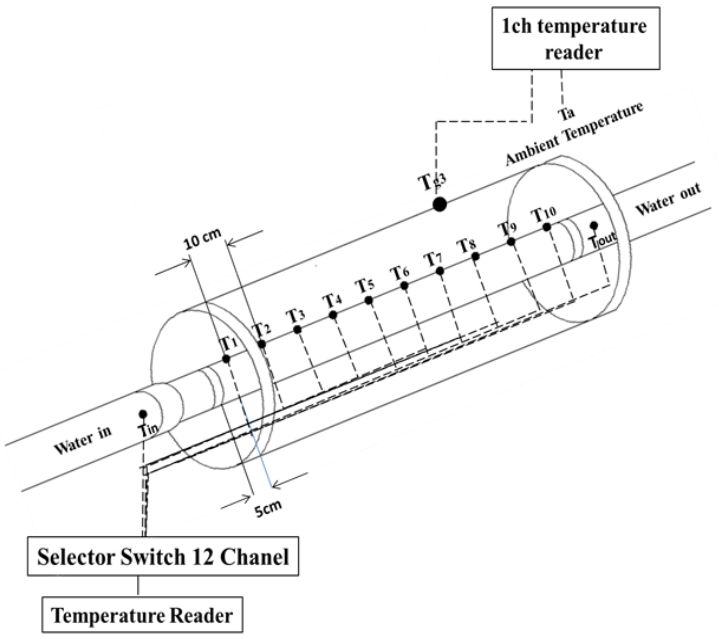

Figure 5. Schematic diagram of thermocouples locations.

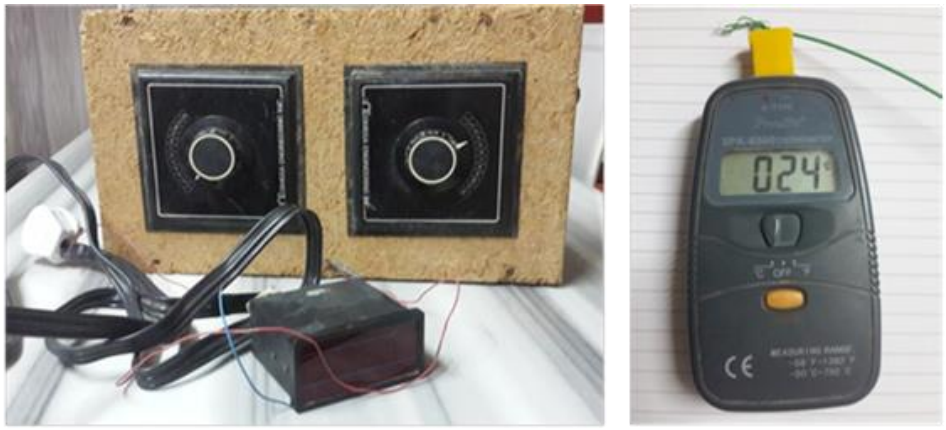

Figure 6. (a)-Selector switch and the temperature reader.
(b)- Pro'sKit 3PK-6500thermometer reader.

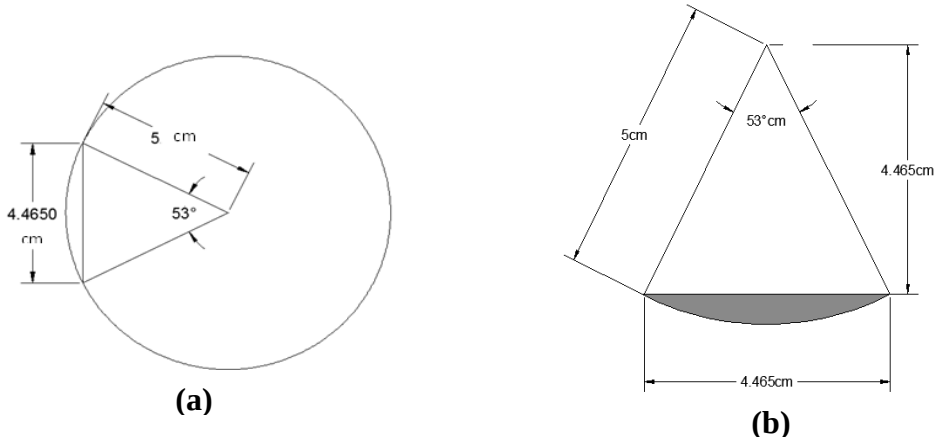

Figure 7. Schematic diagram of (a) lens (b) sector from the lens.

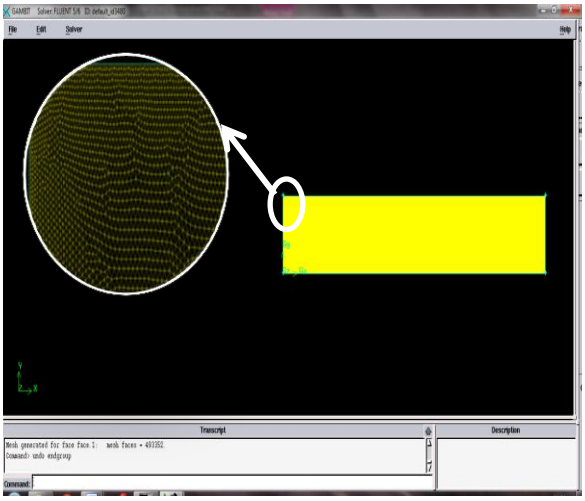

Figure 8. The geometry under the computational mesh.

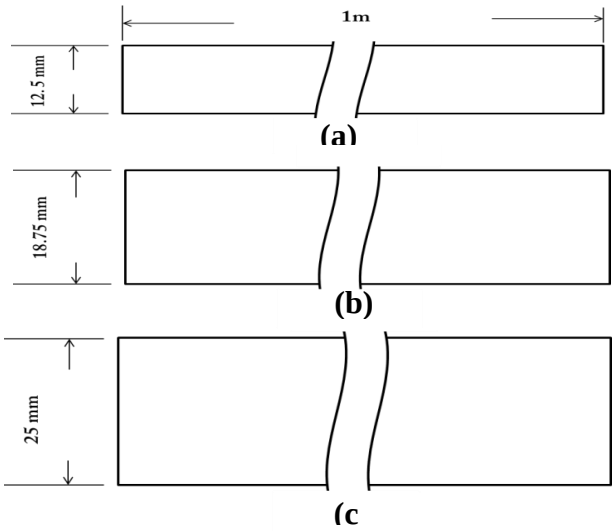

Figure 9. Physical geometry of absorber with diameter of (a) 12.5 mm, (b) 18.75 mm, (c) 25 mm.

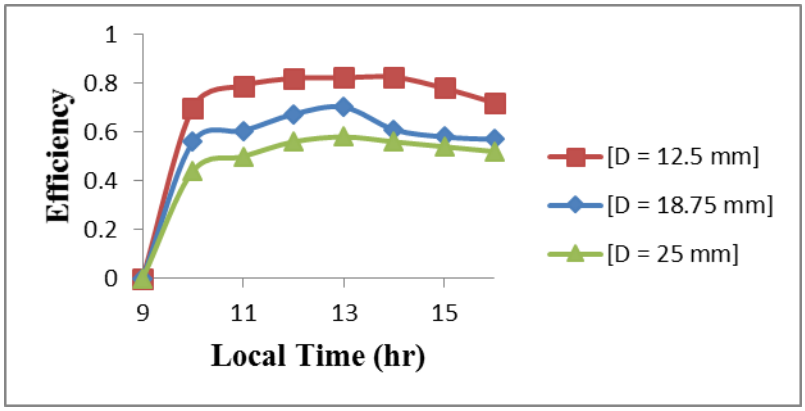

Figure 10. Variation of efficiency with local time for three different absorber diameters.

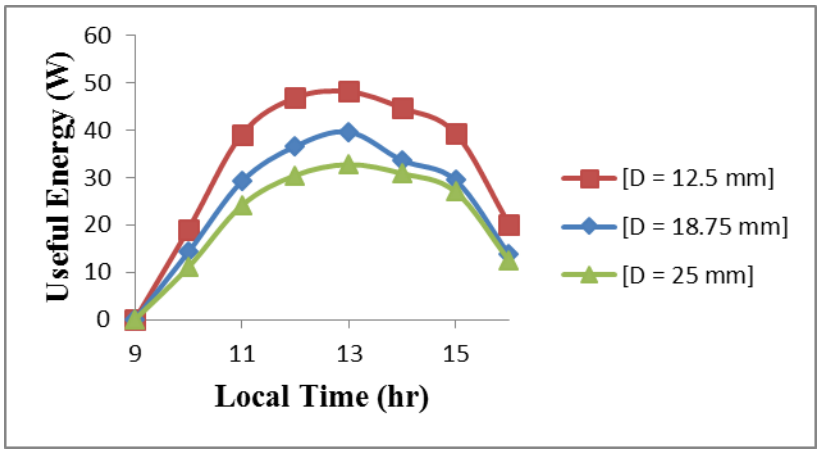

Figure 11. Variation of useful energy with local time for three different absorber diameters.

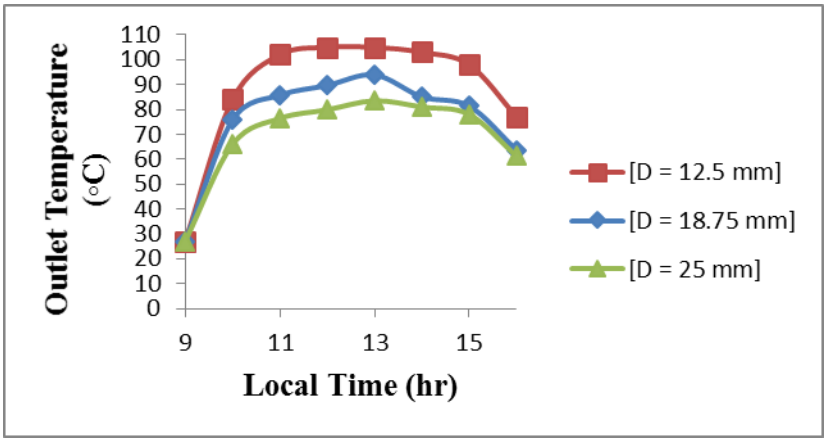

Figure 12. Variation of outlet temperature with local time for three different absorber diameters.

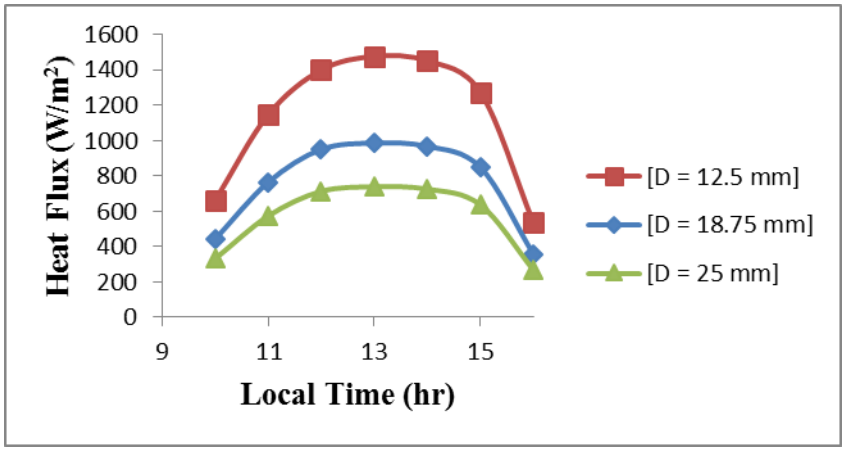

Figure 13. Variation of heat flux with local time for three different absorber diameters.

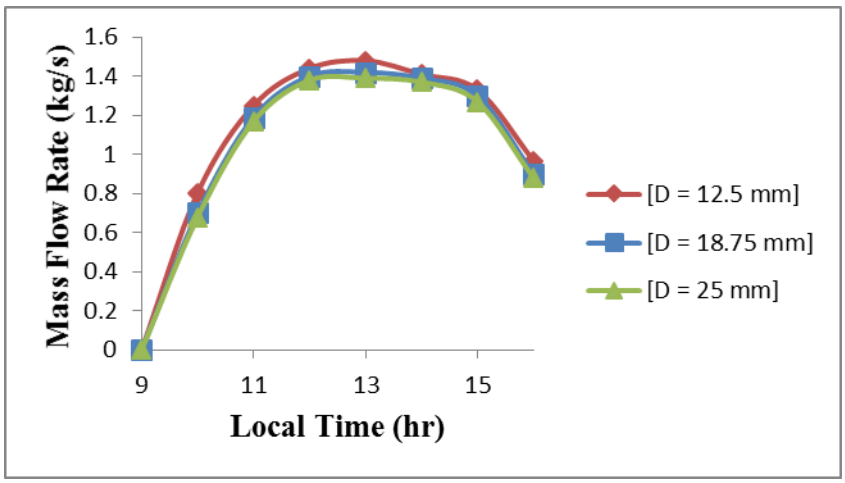

Figure 14. Variation of mass flow rate with local time for three different absorber diameters.

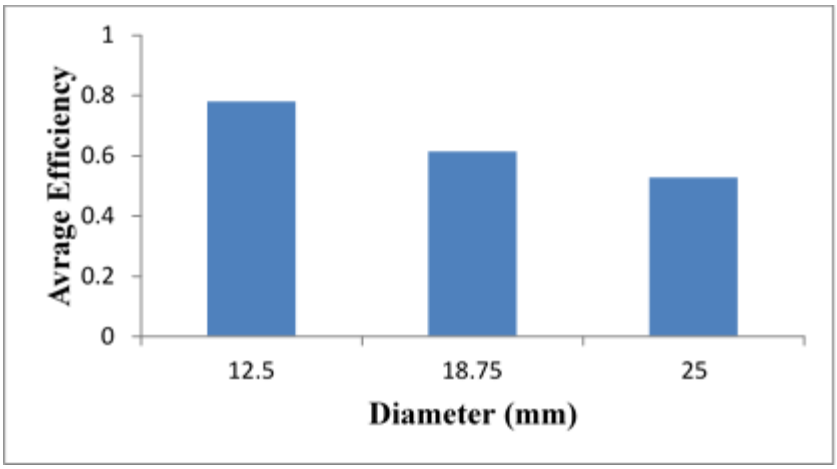

Figure 15. Variation of daily efficiency with absorber diameters on 17th of May 2015.

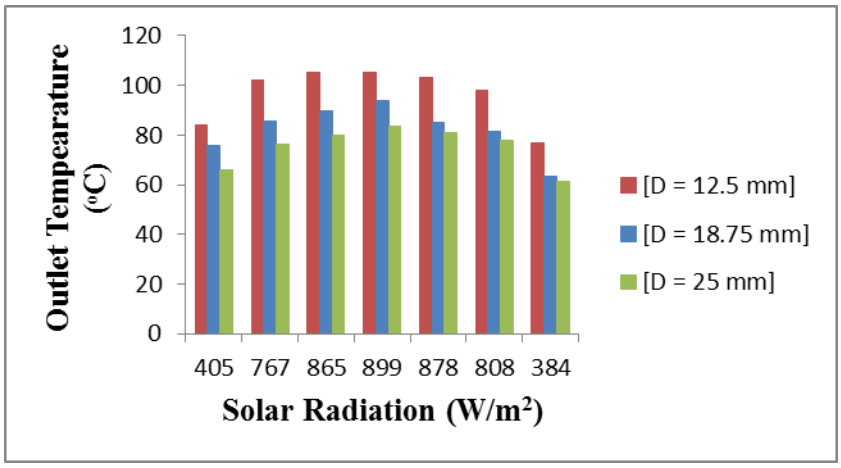

Figure 16. Variation of outlet temperature with solar radiation for three different absorber diameters.

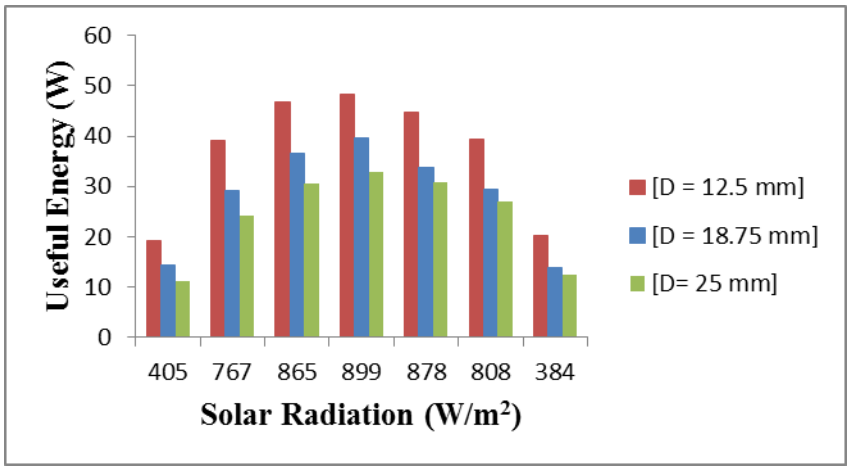

Figure 17. Variation of useful energy with solar radiation for three different absorber diameters.

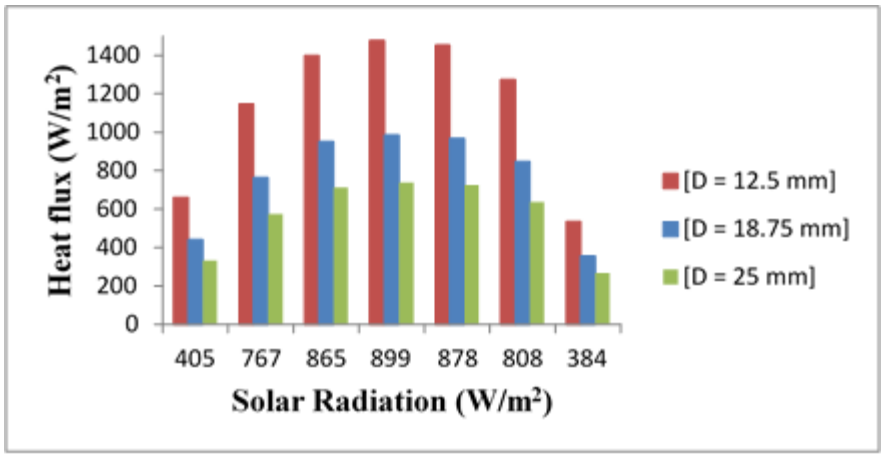

Figure 18. Variation of heat flux with solar radiation for three different absorber diameters.

Table 1. Description of the lens.

Lenses	Description
Appearance	Circle
Diameter size	100 mm
Thickness	5 mm
Focal length	300 mm

Table 2. Boundary conditions of inlet temperature and wall heat flux.

Time (hr)	Inlet Temperature (˚C)	Heat Flux (W/m^2) D=12.5 mm	Heat Flux (W/m^2) D=18.75 mm	Heat Flux (W/m^2) D=25 mm
10:00 AM	27	662	441.6	331.2
11:00 AM	27	1146	764.33	573.24
12:00 PM	27	1400	951	713.3
13:00 PM	27	1478	986.13	738.8
14:00 PM	27	1452	968.26	726.11
15:00 PM	27	1274	849.2	636.9
16:00 PM	27	535	356.68	267.5

NOMENCLATURES

Latin Symbols

Symbol	Description	Symbol	Description
A	area (m^2)	q_b	pool boiling heat transfer (W/m^2)
Cp	specific heat (J/kg. K)	Q_{loss}	heat loss (W)
C	concentration ratio	Q_{useful}	useful heat (W)
D	diameter (m)	Q_{abs}	absorbed heat (W)
F'	collector efficiency factor	Q_u	actual useful heat gain (W)
F''	collector geometry factor	t	time (s)
F_R	collector heat removal factor	T	temperature (K)
$F.R$	fill ratio	$\overline{T}$	average temperature between ambient and sky (K)
Gr	Grashof number	ΔT	temperature difference (K)
g	Gravitational acceleration (m/s^2)	T_a	ambient temperature (K)
h	heat transfer coefficient (W/$m^2.K$)	U_L	overall heat loss coefficient (W/m^2.K)
h_{fg}	latent heat of vaporization (W/$m^2.K$)	U_o	heat loss coefficient based on the outside diameter of the absorber (W/m^2.K)
I_T	solar radiation intensity (W/m^2)	V_w	wind speed (m/s)
k	thermal conductivity (W/m. K)	V_r	flow velocity at r direction (m/s)
L	length of the collector (m)	$V_\emptyset$	flow velocity at $\emptyset$ direction (m/s)
$\dot{m}$	mass flow rate (kg/s)	V_z	flow velocity at z direction (m/s)
Nu	Nusselt number	x	distance along the collector (m)
Pr	Prandtl number		

Greek Symbols

Symbol	Description
$\tau\alpha$	transmittance-absorptance product
ρ	density (kg/m^3)
ϵ	surface tension (N/m)
β	thermal expansion coefficient (K^{-1})
ε_g	emissivity of the glass cover
ε_g	emissivity of the Absorber
μ	dynamic viscosity of the working fluid (Kg/m. s)
σ	Stefan-Boltzmann constant (W/m^2.K^4)
η	efficiency

Subscript

Symbol	Description
1	single-phase region
a	aperture
abs	absorber
abs, cs	absorber cross-sectional
air	air
b	pool boiling region
f	working fluid
g	glass cover
i	inside side
in	inlet
l	liquid-phase
out	outlet
o	outside side
$r, abs-g$	radiation between absorber and glass cover
ref	reference
$r, g-s$	radiation from glass cover to the ambient
sky	sky
sat	saturated
T	total
v	vapor-phase
w	wind
x	local